The Poleward Migration of the Location of Tropical Cyclone Maximum Intensity

James P. Kossin[1], Kerry A. Emanuel[2], and Gabriel A. Vecchi[3]

[1]NOAA National Climatic Data Center, Madison, WI, USA
[2]Program in Atmospheres, Oceans, and Climate, Massachusetts Institute of Technology, Cambridge, MA, USA
[3]NOAA Geophysical Fluid Dynamics Laboratory, Princeton, NJ, USA

*Corresponding author address: James P. Kossin, NOAA/NCDC, University of Wisconsin/CIMSS, 1225 W. Dayton St., Madison, WI 53706 USA. E-mail: james.kossin@noaa.gov

Citation:

Temporally inconsistent and potentially unreliable global historical data hinder detection of trends in tropical cyclone activity[1-3]. This limits the confident evaluation of proposed linkages between observed trends in tropical cyclones and in the environment[4-5]. Here we mitigate this difficulty by focusing on a metric that is comparatively insensitive to past data uncertainty, and we identify a pronounced poleward migration in the average latitude where tropical cyclones have achieved their lifetime-maximum intensity (LMI) over the past 30 years. The poleward trends are evident in the global historical data in both the Northern and Southern Hemispheres with rates of 53 and 62 km decade^{-1}, respectively, and are statistically significant. When considered together, the trends in each hemisphere depict a global-average migration of tropical cyclone activity away from the tropics at a rate of about 1° latitude decade^{-1}, which lies within the range of estimates of the observed expansion of the tropics over this same period[6]. The global migration remains evident and statistically significant under a formal data homogenisation procedure[3] and is unlikely to be a data artefact. The migration away from the tropics is apparently linked to marked changes in the mean meridional structure of environmental vertical wind shear and potential intensity and can be plausibly linked to tropical expansion, which is generally thought to have anthropogenic contributions[6].

Inconsistencies in the historical global "best-track" data can introduce substantial uncertainty into global-mean measures of tropical cyclone activity. Since the introduction of geostationary weather satellites in the mid- to late-1970s, measures of tropical cyclone frequency are generally considered to be accurate, and there is no observed trend in global frequency since that time[7,8]. Comparatively, measures of tropical cyclone intensity are considered to be highly uncertain in the global data[3,9]. Consequently, storm duration is also uncertain because identifying the moment of cyclogenesis requires accuracy in intensity estimates, as the definition of cyclogenesis is entirely dependent on a nascent storm's intensity reaching a formally specified threshold. Similar uncertainty exists in identifying cyclolysis. These uncertainties can project onto metrics such as power dissipation[10] and accumulated cyclone energy[11], which are amalgamations of frequency, duration, and intensity.

But measurements of a storm's position taken around the time that it reaches its lifetime-maximum intensity (LMI) are much less uncertain. By this time in a storm's evolution, it is more likely to have been detected and to be under close observation. Measurements of storm position at the time of LMI are also less sensitive to inaccuracy in measurements of intensity, as well as known inter-regional differences in wind-averaging techniques[9], since determining the *absolute* LMI is not critical, but only that the storm has reached a maximum relative to its lifetime. This also makes measurements of storm position at the time of LMI comparatively insensitive to temporal heterogeneity in the historical best-track intensity record[3]. It is this heterogeneity that has presented substantial challenges to trend detection in tropical cyclone metrics that require absolute measures of intensity[5].

Here we consider the 31-year period 1982–2012, which is the period in which the global best-track data are considered most complete and at their highest quality in each basin[9], and storm position is well-monitored globally by geostationary satellites. This period also encompasses a recent satellite-based global tropical cyclone intensity reanalysis[3], and represents the most reliable period of the atmospheric reanalysis products[12-14] that provide information on the environmental changes that affect tropical cyclones.

When the annual-mean latitude of LMI is calculated from the best-track data in the Northern and Southern hemispheres over this period (Fig. 1a,b, red lines), there are clear and statistically significant poleward trends in both hemispheres of 53 and 62 km decade^{-1}, respectively (Table 1). The positive contribution to these hemispheric trends from each ocean basin except the N. Indian Ocean (Table 1, Extended Data Fig. 1) suggests that the migration away from the tropics is a global phenomenon, although there are large regional differences in the trend amplitudes and their statistical power. These differences are likely due, in part, to regional differences in interannual to multidecadal variability[15]. The largest contribution to the N. Hemisphere trend is from the western N. Pacific, which is also the most active basin in terms of annual tropical cyclone frequency. By contrast, the N. Indian Ocean has the lowest mean annual frequency and the small equatorward trend there has a much lesser effect on the hemispheric trend. The N. Atlantic and eastern N. Pacific exhibit small poleward trends and also contribute little to the hemispheric trend. In the S. Hemisphere, both the S. Pacific and S. Indian Ocean regions contribute substantially to the poleward trend.

Within the period 1982–2009, the latitude of LMI can be reanalyzed using a globally homogenised record of intensity (ADT-HURSAT[3]). When this is done, the annual-mean time series exhibit similar variability and trends (Fig. 1a,b, blue lines), although the ADT-HURSAT-based trend has greater (lesser) amplitude than the best-track-based trend in the N. (S.) Hemisphere (Table 1) and the trend in the S. Hemisphere is no longer significant with 95% confidence. However, when both hemispheres are considered together they depict a global migration away from the deep tropics, and the best-track and ADT-HURSAT data exhibit similar poleward trends of 115 and 118 km decade^{-1}, respectively (Table 1). In this global view, the trends in the best-track and ADT-HURSAT data are consistent and both are statistically significant.

As found with the best-track data, the ADT-HURSAT-based time series exhibit large differences in the trend amplitudes and their statistical power when separated by ocean basin (Table 1, Extended Data Fig. 2). The western N. Pacific is the largest contributor to the trend in the N. Hemisphere and the eastern N. Pacific also contributes significantly, unlike the best-track data from that region. The equatorward trend in the N. Indian Ocean best-track data is not found in the ADT-HURSAT data, which shows essentially no trend in that region (the lack of any poleward trend in the N. Indian Ocean might be expected given the confines of the basin and close proximity of land to the north). In the North Atlantic, the best-track and ADT-HURSAT datasets

both show essentially no trend. There are similar poleward trends in the best-track and ADT-HURSAT data from the South Pacific, but the ADT-HURSAT data in the South Indian Ocean exhibits a smaller, statistically insignificant trend.

Although regional differences are evident, the migration of the mean latitude of LMI away from the deep tropics is observed in both the N. and S. hemispheres, which indicates that this is a global phenomenon. The genesis and subsequent intensification period of tropical cyclones, which precedes LMI and controls when and where LMI occurs, is strongly modulated by the environment that the storms move through in this period. Known major factors controlling tropical cyclone evolution are the environmental vertical wind shear and the potential intensity[16-18]. Potential intensity (PI) describes the thermodynamically-based maximum tropical cyclone intensity that the environment will support, all other factors being optimal. Vertical wind shear is one of the key factors that inhibits a storm from achieving this maximum. Greater shear and lesser PI each inhibit genesis and intensification and vice versa, and thus increased shear in the deep tropics and/or decreased shear at higher latitudes can be plausibly linked to a poleward migration of the latitude of LMI. Decreased PI in the deep tropics and/or increased PI at higher latitudes could be expected to result in a similar migration. Here we explore these environmental factors using three different atmospheric reanalysis products, NCEP/NCAR[12], ERA-Interim[13], and MERRA[14]. All three products exhibit broad regions of increased shear in the deep tropics and decreased shear in the subtropics (Fig. 2), which is consistent with the observed changes in the tropical cyclones. The changes in mean PI are not as uniformly consistent among the different reanalysis products, particularly in the tropics, which is likely due to spurious differences in upper tropospheric temperatures[19,20], but the meridional structure of PI change is generally consistent in showing greater increases at higher latitudes, and the MERRA data in particular also show a broad reduction of potential intensity in the deep tropics.

The observed changes in shear and potential intensity provide evidence that the global migration of tropical cyclones away from the tropics is being modulated by systematic environmental changes. Shifts in tropical cyclone tracks in most regions have also been linked to phase changes in the El Niño–Southern Oscillation[21-24] (ENSO), which can potentially contribute to the poleward trends in LMI identified here. To test this, we diminish the contribution of ENSO by regressing the latitude of LMI time series onto an index of ENSO variability. When this is done (Fig. 3), the amplitude of the interhemispheric migration rates are found to decrease only slightly in both the best-track and ADT-HURSAT data, and in fact the statistical power of the trends increases. This makes it unlikely that natural ENSO variability is playing a role in the observed multidecadal poleward migration of LMI although it plays a substantial role in its interannual variability.

The potential for contributions from natural variability occurring on decadal or longer time-scales still exists, but quantifying this is always difficult with relatively short observation records. We hypothesise that there is a linkage between the poleward migration of LMI and the observed

expansion of the tropics. The rate of expansion since 1979 varies considerably among existing studies[6], but the rate of LMI migration identified here falls well within this range. This potential linkage between tropical cyclones and the expansion of the tropics further heightens interest in establishing the forcing mechanisms of the expansion, which are presently uncertain but generally thought to have anthropogenic contributions[6]. The expansion of the tropics, as measured by the meridional extent of the tropical Hadley circulation, exhibits a step-change in the late 1990s[6]. Formal change-point analysis applied to the global time series of LMI latitude reveals a significant change-point in 1996, providing further support for a linkage between the two independently-observed phenomena.

Observed changes in vertical wind shear and potential intensity over the past 30-years appear to have resulted in a poleward shift in both the N. and S. hemispheres of the regions most favourable for tropical cyclone development (Fig. 2), and an associated migration of tropical cyclone activity away from the tropics (Fig. 1). If these environmental changes continue, a concomitant continued poleward migration of the latitude where tropical cyclones achieve their LMI would have potentially profound consequences to life and property. Any related changes to positions where storms make landfall will have obvious effects on coastal residents and infrastructure. Increasing hazard exposure and mortality risk from tropical cyclones[25] may be compounded in coastal cities outside of the tropics, while possibly being offset at lower latitudes. Tropical cyclones also play an important role in maintaining regional water resources[26,27] and a poleward migration of storm tracks can threaten potable water supplies in some regions while increasing flooding events in others. Given these motivating factors, further study of the poleward migration of tropical cyclone LMI identified here and its potential link to the observed expansion of the tropics is warranted.

Methods Summary: Best-track data were taken from the International Best Track Archive for Climate Stewardship (IBTrACS) v03r05 (ref. 28). Following ref. 3, when a storm has overlapping data from multiple sources, the source with the greatest reported LMI is used. The homogenised intensity data were taken from the Advanced Dvorak Technique-Hurricane Satellite (ADT-HURSAT) dataset described in ref. 3. Vertical wind shear and potential intensity were calculated over water in the region spanning 35°S–35°N latitude. In the S. Hemisphere, the longitude was confined to 30–240°E longitude, which excludes the region where storms are not observed to form or track. The wind shear is estimated as the magnitude of the vector difference of the horizontal wind at the 250 and 850 hPa pressure levels. Potential intensity was calculated following ref. 29. ENSO variability was diminished from the latitude of LMI time series by regressing the series from the N. and S. Hemispheres onto the Niño-3.4 index[30] averaged over the most active periods of tropical cyclone activity [Aug–Oct (Jan–Mar) in the N. (S.) Hemisphere], and analyzing the residuals. None of the time series explored in this paper exhibited autocorrelation after detrending, as determined with the Durbin-Watson test statistic, and no corrections were necessary when calculating the confidence intervals.

References

1. Landsea, C. W., Vecchi, G. A., Bengtsson, L. & Knutson, T. R. Impact of duration thresholds on Atlantic tropical cyclone counts. *J. Clim.*, **23**, 2508–2519 (2010).
2. Vecchi, G. A. & Knutson, T. R. Estimating annual numbers of Atlantic hurricanes missing from the HURDAT database (1878-1965) using ship track density. *J. Clim.*, **24**, 1736-1746 (2011).
3. Kossin, J. P., Olander, T. L. & Knapp, K. R. Trend analysis with a new global record of tropical cyclone intensity. *J. Clim.*, **26**, 9960-9976. (2013).
4. Knutson, T. R., McBride, J. L., Chan, J., Emanuel, K., Holland, G., Landsea, C., Held, I., Kossin, J. P., Srivastava, A. K. & Sugi, M. Tropical cyclones and climate change. *Nature Geoscience*, **3**, doi:10.1038/ngeo779 (2010).
5. Seneviratne, S. I. & coauthors. Changes in climate extremes and their impacts on the natural physical environment. In: *Managing the Risks of Extreme Events and Disasters to Advance Climate Change Adaptation* [Field, C. B., V. Barros, T. F. Stocker, D. Qin, D. J. Dokken, K. L. Ebi, M. D. Mastrandrea, K. J. Mach, G. -K. Plattner, S. K. Allen, M. Tignor, and P. M. Midgley (eds.)]. A Special Report of Working Groups I and II of the Intergovernmental Panel on Climate Change (IPCC). Cambridge University Press, Cambridge, UK, and New York, NY, USA, pp. 109-230 (2012).
6. Lucas, C., Timbal, B. & Nguyen, H. The expanding tropics: a critical assessment of the observational and modeling studies. *WIREs Clim. Change*, **5**, 89–112 (2014).
7. Frank, W. M & Young, G. S. The interannual variability of tropical cyclones. *Mon Wea. Rev*, **135**, 3587–3598 (2007).
8. Holland, G. & Bruyere, C.L. Recent intense hurricane response to global climate change. *Climate Dynamics*, DOI: 10.1007/s00382-013-1713-0 (2013).
9. Knapp, K. R. & Kruk, M. C. Quantifying interagency differences in tropical cyclone best track wind speed estimates. *Mon. Wea. Rev.*, **138**, 1459-1473 (2010).
10. Emanuel, K. A. Increasing destructiveness of tropical cyclones over the past 30 years. *Nature*, **436**, 686-688 (2005).
11. Bell, G. D. & coauthors. Climate assessment for 1999. *Bull. Am. Meteorol. Soc.*, **81**, s1–s50, doi:10.1175/1520-0477 (2000).
12. Kalnay, E. & coauthors. The NCEP/NCAR 40-year reanalysis project, *Bull. Am. Meteorol. Soc.*, **77**, 437-470 (1996).
13. Dee, D.P. & Coauthors. The ERA-Interim reanalysis: configuration and performance of the data assimilation system, *Q. J. R. Meteorol. Soc.*, **137**, 553-597 (2011).
14. Rienecker, M. & Coauthors. MERRA: NASA's Modern-Era Retrospective Analysis for Research and Applications, *J. Clim.*, **24**, 3624-3648, doi: 10.1175/JCLI-D-11-00015.1 (2011).
15. Bindoff, N.L. & coauthors.2013: Detection and Attribution of Climate Change: from Global to Regional. In: Climate Change 2013: The Physical Science Basis. Contribution of Working Group I to the Fifth Assessment Report of the Intergovernmental Panel on Climate Change [Stocker, T.F., D. Qin, G.-K. Plattner, M. Tignor, S.K. Allen, J. Boschung, A. Nauels, Y. Xia, V. Bex and P.M. Midgley (eds.)]. Cambridge University Press, Cambridge, United Kingdom and New York, NY, USA (2013).
16. Knaff, J. A., Seseske, S. A., DeMaria, M. & Demuth, J. L. On the influences of vertical wind shear on symmetric tropical cyclone structure derived from AMSU. *Mon. Wea. Rev.*, **132**, 2503–2510 (2004).

17. Zhang, F. & Tao, D. Effects of vertical wind shear on the predictability of tropical cyclones. *J. Atmos. Sci.*, **70**, 975–983. doi: http://dx.doi.org/10.1175/JAS-D-12-0133.1 (2013).

18. Emanuel, K. A. Thermodynamic control of hurricane intensity. *Nature*, **401**, 665-669 (1999).

19. Vecchi, G. A., Fueglistaler, S., Held, I. M., Knutson, T. R. & Zhao, M. Impacts of atmospheric temperature trends on tropical cyclone activity. *J. Clim.*, **26**, 3877–3891 (2013).

20. Emanuel, K., Solomon, S., Folini, D., Davis, S. & Cagnazzo, C. Influence of tropical tropopause layer cooling on Atlantic hurricane activity. *J. Clim.*, **26**, 2288–2301 (2013).

21. Camargo, S. J., Robertson, A. W., Gaffney, S. J., Smyth, P & and Ghil, M. Cluster analysis of typhoon tracks. Part II: Large-scale circulation and ENSO. *J. Clim.*, **20**, 3654–3676 (2007).

22. Camargo, S. J., Robertson, A.W., Barnston, A. G. & Ghil, M. Clustering of eastern North Pacific tropical cyclone tracks: ENSO and MJO effects. *Geochemistry, Geophysics and Geosystems*, **9**, Q06V05, doi: 10.1029/2007GC001861 (2008).

23. Kossin, J. P., Camargo, S. J. and Sitkowski, M. Climate modulation of North Atlantic hurricane tracks. *J. Clim.*, **23**, 3057-3076 (2010).

24. Ramsay, H. A., Camargo, S. J. & Kim, D. Cluster analysis of tropical cyclone tracks in the Southern Hemisphere. *Climate Dynamics*, **39**, 897-917 (2012).

25. Peduzzi, P., Chatenoux, B., Dao, H., De Bono, A., Herold, C., Kossin, J., Mouton, F. & Nordbeck, O. Tropical cyclones: Global trends in human exposure, vulnerability and risk. *Nature Climate Change*, **2**, 289-294 (2012).

26. Jiang, H. & Zipser, E. Contribution of tropical cyclones to the global precipitation from eight seasons of TRMM data: Regional, seasonal, and interannual variations. *J. Clim.*, **23**, 1526–1543 (2010).

27. Lam, H., Kok, M. H. & Shum, K. K. Y. Benefits from typhoons – the Hong Kong perspective. *Weather*, **67**, 16-21 (2012).

28. Knapp, K. P., Kruk, M. C., Levinson, D. H., Diamond, H. J. & Neumann, C. J. The International Best Track Archive for Climate Stewardship (IBTrACS): unifying tropical cyclone data. *Bull. Am. Meteorol. Soc.* **91**, 363–376 (2010).

29. Bister, M. & Emanuel, K. A. Dissipative heating and hurricane intensity. *Meteorol. Atmos. Phys.*, **65**, 233–240 (1998).

30. Barnston, A. G., M. Chelliah, and S. B. Goldenberg, 1997: Documentation of a highly ENSO-related SST region in the equatorial Pacific. *Atmos.–Ocean,* 35, 367–383.

Author Contributions: J.P.K. conceived of and designed the study, and performed the analyses with input from K.A.E and G.A.V., J.P.K., K.A.E, and G.A.V. provided data and participated in interpretation of the results and the writing of the manuscript.

Author Information Reprints and permissions information is available at www.nature.com/reprints. The authors declare no competing financial interests. Readers are welcome to comment on the online version of the paper. Correspondence and requests for materials should be addressed to J.P.K. (james.kossin@.noaa.gov).

Table 1 | Linear trends, by region, of annual-mean latitude of LMI.

	NHEM	SHEM	NATL	WPAC	EPAC	NIO	SIO	SPAC	GLBL
Best-track	+53±43	+62±48	+7±98	+37±55	+10±32	−25±78	+67±55	+51±68	+115±70
ADT-HURSAT	+83±50	+35±44	−12±126	+105±71	+34±30	+10±106	+30±52	+54±79	+118±70

The regions are, left to right, Northern and Southern Hemispheres, N. Atlantic, western and eastern N. Pacific, N. and S. Indian Oceans, S. Pacific, and Global. Trends are deduced from the best-track (top row) and ADT-HURSAT (bottom row) datasets. The slope (in km decade^{-1}) and the 95% two-sided confidence bounds are shown in each region. Positive slopes represent poleward migration.
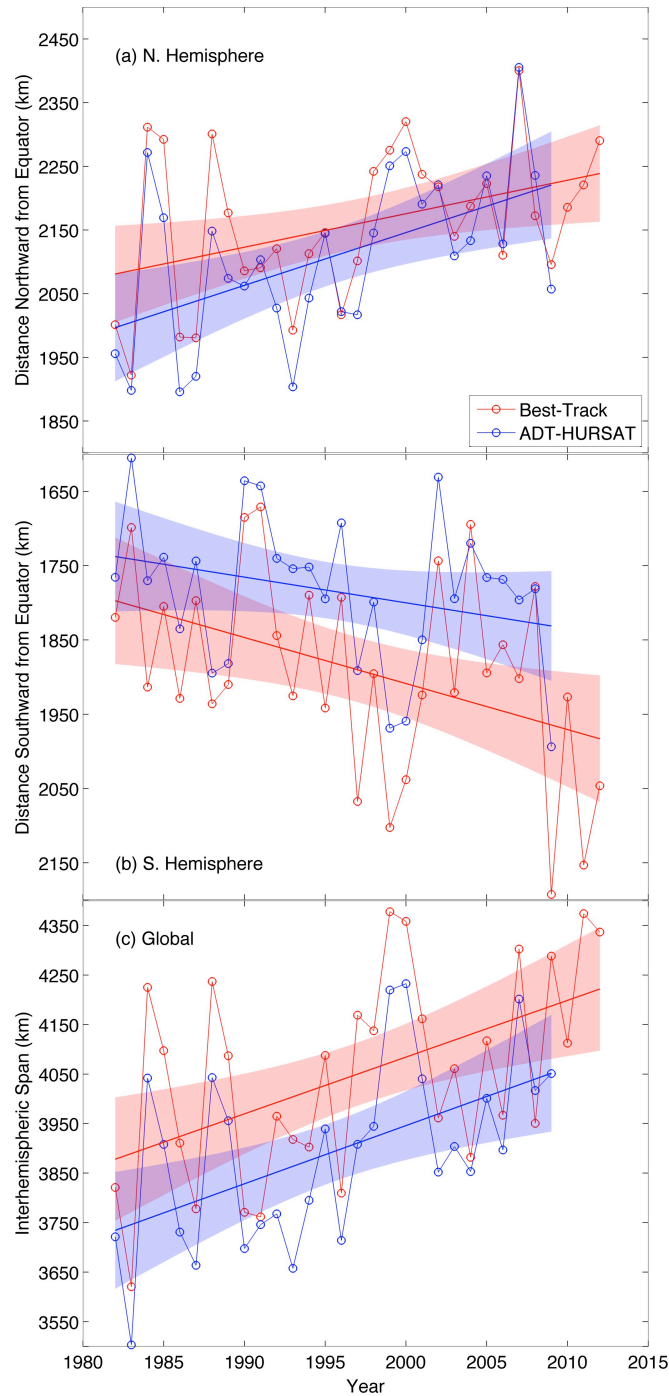
Figure 1 | Poleward migration of the latitude of lifetime-maximum intensity (LMI) away from the tropics. Time series of annual-mean latitude of tropical cyclone LMI calculated from the best-track historical data (red) and the ADT-HURSAT reanalysis (blue) in the Northern (**a**) and Southern (**b**) Hemispheres, and the annual-mean difference between them (**c**) depicting the global migration of the latitude of LMI away from the tropics. Linear trend lines are shown with their 95% two-sided confidence intervals (shaded). Note that the y-axis in (**b**) increases downwards.
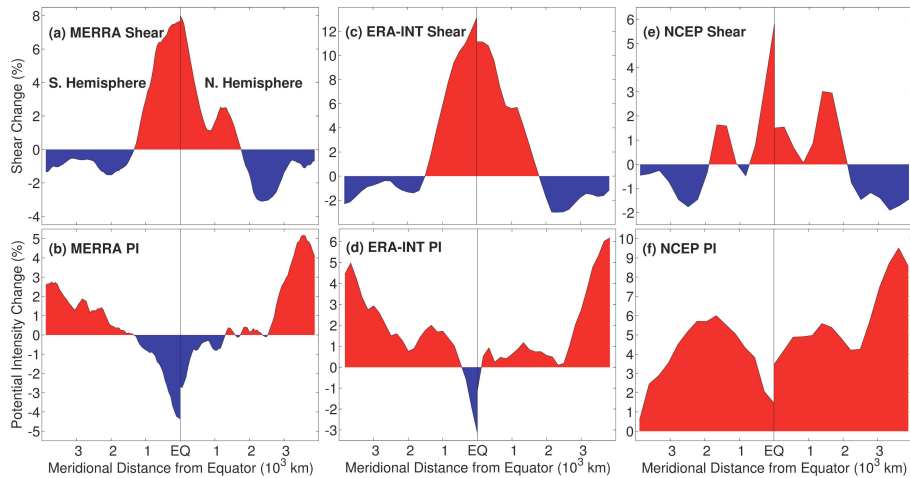
Figure 2 | Observed changes in the mean environment where tropical cyclones form and track. Percent changes from the period 1980–1994 to 1995–2010 in mean vertical wind shear (**a**, **c**, **e**) and potential intensity (**b**, **d**, **f**). Annual-means are taken over the peak tropical cyclone seasons in each hemisphere (Aug–Oct in N. hemisphere, Jan–Mar in S. Hemisphere) from three different reanalysis products MERRA (**a**, **b**), ERA-Interim (**c**, **d**), and NCEP/NCAR (**e**, **f**).
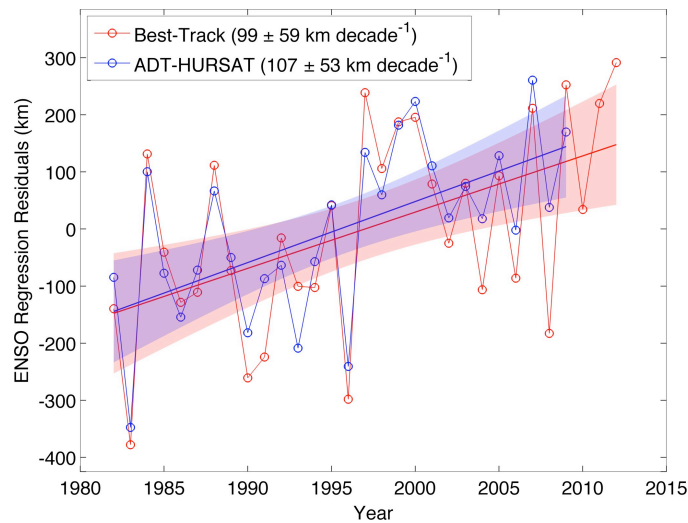

Figure 3 | Global trends of the latitude of LMI with ENSO variability reduced. Time series of the latitude of LMI calculated from the best-track historical data (red) and the ADT-HURSAT reanalysis (blue) with ENSO variability reduced. The values are calculated from residuals of the regression of latitude of LMI onto an index of ENSO variability. Shading represents the 95% two-sided confidence interval of the trend.

Methods

Best-track data were taken from the International Best Track Archive for Climate Stewardship (IBTrACS) v03r05 (ref. 28) and are available at http://www.ncdc.noaa.gov/ibtracs/. Following ref. 3, when a storm has overlapping data from multiple sources, the source with the greatest reported LMI is used. In storms that achieve their LMI more than once, the latitude of LMI is taken at the first occurrence. The homogenised intensity data were taken from the Advanced Dvorak Technique-Hurricane Satellite (ADT-HURSAT) dataset described in ref. 3 (available by request from J.P.K.). The data reflect the additional homogenisation procedure addressing the discontinuity in satellite coverage ca. 1997. The global distribution of the ADT-HURSAT LMI is known to be spuriously leptokurtic[3], which is the likely cause of the consistent equatorward bias in the mean latitude of LMI when compared to the best-track, but there is no expectation that this bias has any time dependence and is not expected to affect the trends.

ENSO variability was removed from the latitude of LMI time series by regressing the individual series from the N. and S. Hemispheres onto the Niño-3.4 index[30] averaged over the most active periods of tropical cyclone activity [Aug–Oct (Jan–Mar) in the N. (S.) Hemisphere], and analyzing the residuals. The index is available at http://www.cpc.ncep.noaa.gov/data/indices/.

None of the time series explored in this paper exhibit autocorrelation after detrending, as determined with the Durbin-Watson test statistic, and no corrections were necessary when calculating the confidence intervals. In addition to linear trend analysis, the time series were explored for change-points with models based on batch detection using both the Student-t and Mann-Whitney statistics to test for significance at 95% confidence or greater using the "cpm" package (http://cran.r-project.org/web/packages/cpm/index.html)[31] in the software environment R.

The global trends in the annual mean latitude of LMI are a result of both intra-basin and inter-basin changes. The climatological mean latitude of LMI varies by basin (see, e.g., Extended Data Fig. 1) so that in addition to meridional shifts within each basin, changes in the relative annual frequency of storms from each basin can also contribute to the global trends in the latitude of LMI. To quantify this contribution, the latitude of LMI of every storm was normalised by the respective basin-mean latitude of LMI, and the analysis of Fig. 1c was repeated. When this was performed, the trend in the best-track data decreased from 115 ± 70 to 78 ± 66 km decade^{-1} and the trend in the ADT-HURSAT data decreased from 118 ± 70 to 92 ± 65 km decade^{-1}. Thus both factors contribute, but the intra-basin poleward migration of LMI dominates the trends.
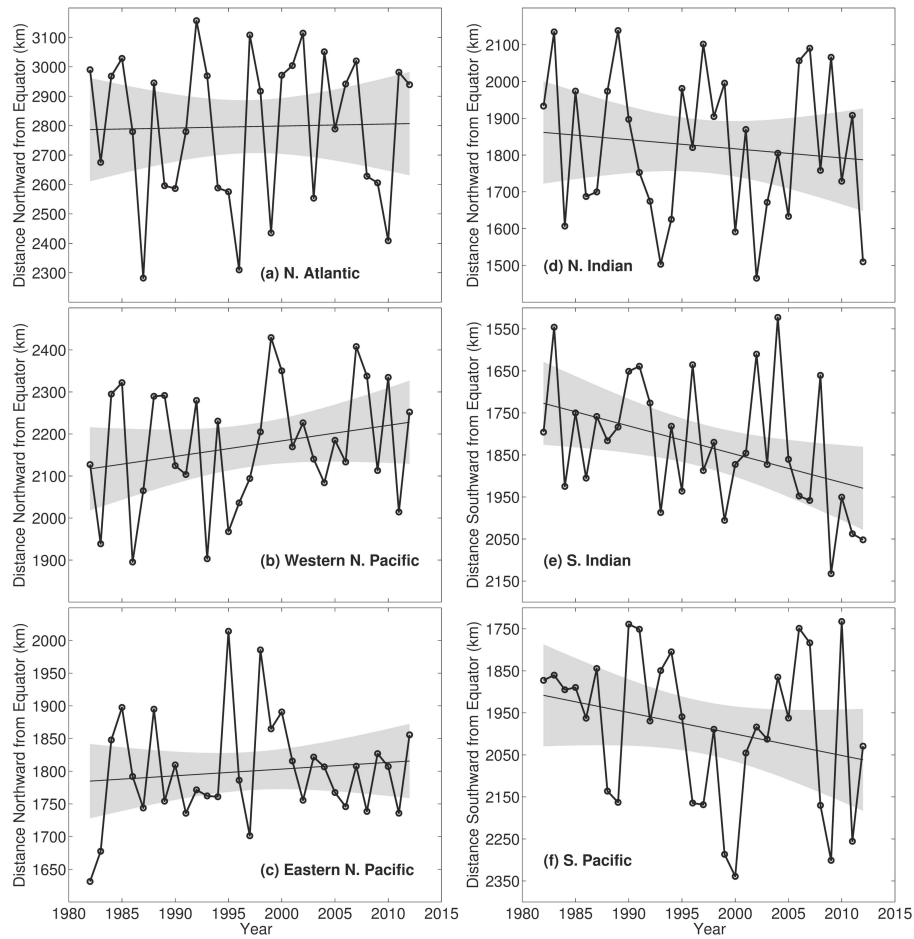
Monthly-mean vertical wind shear and potential intensity (PI) were calculated over water in the region spanning 35°S–35°N latitude. In the S. Hemisphere, the longitude was confined to 30–240°E longitude, which excludes the region where storms are not observed to form or track. Vertical wind shear was calculated following ref. 32, as

$$\text{shear} = \sqrt{(\bar{u}_{250} - \bar{u}_{850})^2 + (\bar{v}_{250} - \bar{v}_{850})^2 + \overline{u'_{250}u'_{250}} + \overline{v'_{250}v'_{250}} + \overline{u'_{850}u'_{850}} + \overline{v'_{850}v'_{850}} - 2(\overline{u'_{250}u'_{850}} + \overline{v'_{250}v'_{850}})}$$
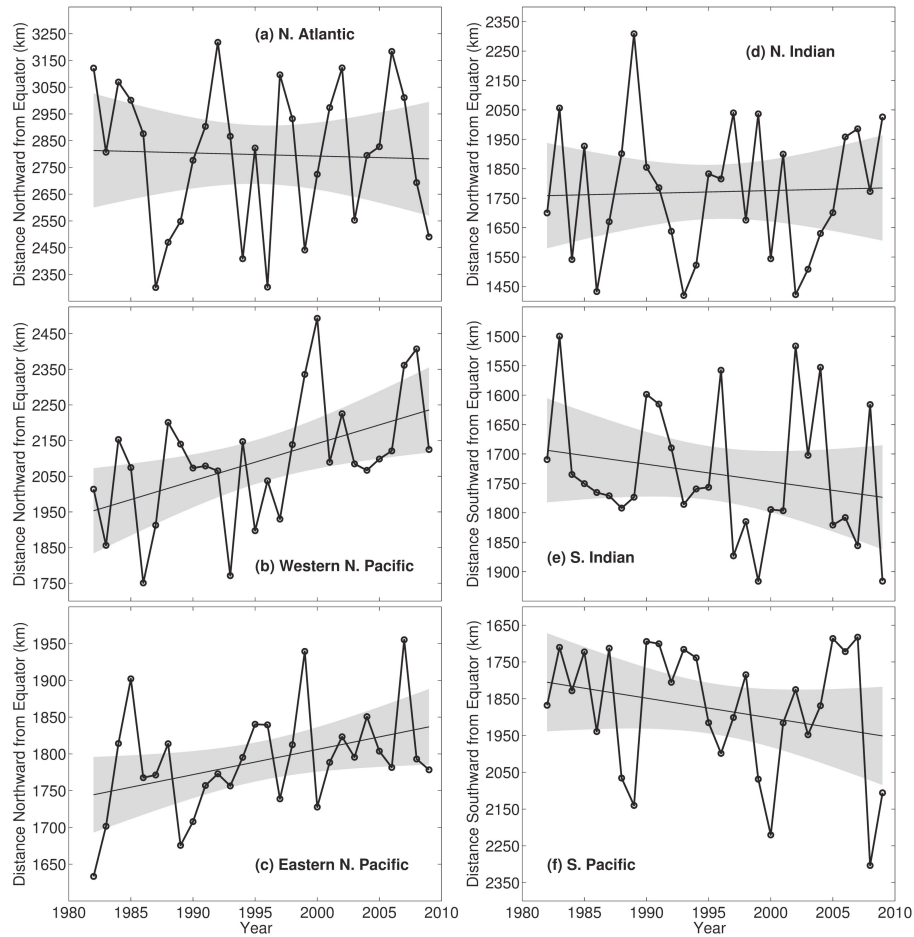
where u_{250}, u_{850}, v_{250}, and v_{850} are the zonal and meridional winds at the 250 and 850 hPa pressure levels, u'_{250}, u'_{850}, v'_{250}, and v'_{850} are departures of daily means from their monthly means, and overbars represent monthly-averaged quantities. PI was calculated following ref. 29. In the N. (S.) Hemisphere, the shear and PI were averaged over Aug–Oct (Jan–Mar).

Methods References

31. Ross, G. J. cpm: Sequential parametric and nonparametric change detection. R package version 1.1. http://CRAN.R-project.org/package=cpm (2013).
32. Emanuel, K. Tropical cyclone activity downscaled from NOAA-CIRES reanalysis, 1908-1958. *J. Adv. Model. Earth Syst*., **2**, doi:10.3894/JAMES.2010.2.1 (2010).

Extended Data Figure 1 | Time series of annual-mean latitude of LMI calculated from the best-track historical data from each ocean basin. The basins are (**a**) North Atlantic, (**b**) western North Pacific, (**c**) eastern North Pacific, (**d**) Northern Indian Ocean, (**e**) Southern Indian Ocean, and (**f**) South Pacific. Linear trend lines are shown with their 95% two-sided confidence intervals (shaded). Note that the y-axes in (**e**) and (**f**) increase downwards.

Extended Data Figure 2 | Time series of annual-mean latitude of LMI calculated from the ADT-HURSAT data from each ocean basin. The basins are (**a**) North Atlantic, (**b**) western North Pacific, (**c**) eastern North Pacific, (**d**) Northern Indian Ocean, (**e**) Southern Indian Ocean, and (**f**) South Pacific. Linear trend lines are shown with their 95% two-sided confidence intervals (shaded). Note that the y-axes in (**e**) and (**f**) increase downwards.